Mechanics of Advanced Materials and Structures

ISSN: (Print) (Online) Journal homepage: www.tandfonline.com/journals/umcm20

Surface Green's functions of a horizontally graded elastic half-plane

Lizichen Chen & Weiqiu Chen

To cite this article: Lizichen Chen & Weiqiu Chen (2024) Surface Green's functions of a horizontally graded elastic half-plane, Mechanics of Advanced Materials and Structures, 31:27, 9601-9610, DOI: 10.1080/15376494.2024.2342042

To link to this article: https://doi.org/10.1080/15376494.2024.2342042

Published online: 14 Apr 2024.

MECHANICS OF ADVANCED MATERIALS AND STRUCTURES
2024, VOL. 31, NO. 27, 9601–9610
https://doi.org/10.1080/15376494.2024.2342042

Taylor & Francis
Taylor & Francis Group

ORIGINAL ARTICLE

Surface Green's functions of a horizontally graded elastic half-plane

Lizichen Chen[a] and Weiqiu Chen[a,b,c]

[a]Key Laboratory of Soft Machines and Smart Devices of Zhejiang Province, Department of Engineering Mechanics, Soft Matter Research Center, Zhejiang University, Hangzhou, P.R. China; [b]Center for Soft Machines and Smart Devices, Huanjiang Laboratory, Zhuji, P.R. China; [c]Faculty of Mechanical Engineering and Mechanics, Ningbo University, Ningbo, P.R. China

ABSTRACT

High-throughput mechanical testing based on functionally graded specimens is very promising for accelerating the development of new materials. However, due to the inhomogeneity-induced complexity, most existing analyses on functionally graded materials have recourse to numerical methods to predict their mechanical responses in reaction to external stimuli. This work investigates the surface Green's functions for an inhomogeneous half-plane with horizontal exponential material gradient subject to both normal and tangential concentrated forces acting on the surface. The governing equations are first simplified by introducing appropriate potential functions, which facilitates the mathematical derivation of displacements *via* the Fourier transform technique. In the case of normal force, the vertical surface displacement is derived explicitly under the weak gradient assumption while the horizontal surface displacement is derived directly without the same assumption. In particular, the Meijer G-function and Fox H-function are introduced to express and simplify the vertical displacement. In the case of tangential force, the analytical expressions of surface displacements are also derived similarly. It is noted that the surface Green's functions not only exhibit singularity and asymmetry properties as expected, but also can be reduced to the classical Boussinesq-Flamant solutions for a homogeneous half-plane. In addition, the analytical results are verified through comparison with the finite element analyses. The surface Green's functions derived here could be a theoretical basis for developing high-throughput mechanical testing methods which use specimens made of functionally graded materials.

ARTICLE HISTORY
Received 8 April 2024
Accepted 8 April 2024

KEYWORDS
functionally graded specimen; surface Green's function; inhomogeneous half-plane; fourier transform; weak gradient assumption; high-throughput mechanical testing

1. Introduction

High-throughput characterization (HTC) of materials has been shown to be effective in accelerating the development and application of materials. Therefore, it has been listed as one of the three major technical elements of the Materials Genome Initiative [1, 2]. A major breakthrough in HTC is the use of specimens made of functionally graded materials (FGMs), which enables a highly time-efficient and space-compact method for material characterization [3]. However, there is still an obvious gap between theoretical analysis and experimental testing, i.e. no rigorous theory (like the classical Hertzian contact theory for homogenous and isotropic materials) has been developed to guide the material characterization based on FGM specimens that are usually inhomogeneous along the horizontal direction. Almost all the current efforts are qualitatively, not quantitatively.

The difficulty of developing theoretical models lies in material inhomogeneity, making the governing equations more complex to be solved analytically [4]. Nevertheless, mechanics of FGMs has been a hot topic in solid mechanics since 1980s due to their various superiorities in applications [5]. In particular, the potential applications of FGMs in mitigating contact related failure have been a catalyst for the swift progress of contact mechanics of FGMs. Over the last three decades, both analytical and experimental studies have indicated that utilizing FGMs for surface coatings can significantly improve the resistance to contact related damage and crack resulting from indentation, frictional sliding, and fretting [6–9].

Before the widespread attention garnered by contact analysis of FGMs, researches on the mechanical properties of gradient materials already exist, primarily focusing on geological materials [10–13], in which the material gradient was considered to vary exponentially or in power-law in depth (i.e. in vertical direction). A series of problems with the action of line and point loads on the surface of geological materials were solved. De Pater and Kalker assumed the Poisson's ratio varies with depth and studied contact problems related to sliding and rolling [14]. For the materials with power-law gradient, Giannakopoulos and Suresh considered the contact problems of a graded elastic half-space with the action of point force and frictionless axisymmetric indenters [15, 16]. Giannakopoulos and Pallot conducted the contact analysis of an FGM half-plane with a frictional rigid indenter [17]. Markus Heß derived closed-form analytical solutions under arbitrary unidirectional tangential loading [18]. For the materials with exponential gradient, Guler and

CONTACT Weiqiu Chen chenwq@zju.edu.cn Key Laboratory of Soft Machines and Smart Devices of Zhejiang Province, Department of Engineering Mechanics, Soft Matter Research Center, Zhejiang University, Hangzhou 310027, P.R. China.

Erdogan studied the contact problems of an elastic half-plane with a surface gradient layer and took account of friction in the contact analyses [19–21]. Ke and Wang proposed a more general model, which involves selecting appropriate discrete layers and utilizing linear approximation of the Young's modulus in the depth direction [22]. Chen et al. investigated the adhesive contact problems of a power-law graded half-space with a rigid spherical indenter [23, 24]. Guo and his collaborators analyzed the adhesive contact problems of a power-law graded half-space with a rigid indenter under both normal and tangential loads [25–27]. In terms of contact analyses with multi-field coupling, Çömez examined continuous and discontinuous contact problems between a graded piezoelectric layer and a homogeneous piezoelectric half-plane under mechanical and electrical loads [28].

However, existing researches mostly focus on the problems of materials with gradient in the vertical direction, and there are few studies on the horizontally graded materials, let alone analytical closed-form solutions. For instance, Dag and his collaborators derived the analytical solutions by solving the stress integral equation for FGMs under the action of a rigid punch of an arbitrary profile, and designed the corresponding finite element algorithms for numerical solutions [29–31]. Notwithstanding the complexity, numerous mathematical methods remain at our disposal for tackling intricate problems, wherein the Green's functions offer a powerful mathematical framework for providing fundamental solutions to boundary-value problems in solid mechanics, especially mixed boundary-value problems encountered in such as contact analyses.

This article focuses on the deformation of an elastic half-plane with exponential material gradient in the horizontal direction subject to point forces applied on the surface. The solutions correspond to the surface Green's functions, which can be used in contact analysis of these FGMs. Surface vertical and horizontal displacements are derived analytically under the action of normal concentrated force in Section 2.1. It is worth noting that the closed-form solution for surface displacement in the vertical direction is obtained under the assumption of weak gradient. While, in the horizontal direction, it is derived in a more straightforward way without the need of introducing the above assumption. Moreover, the vertical surface displacement is further simplified by making use of some special functions. For the tangential concentrated force, the solutions are provided similarly in Section 2.2. Finite element analyses are performed in Section 3 to verify the correctness of the derived analytical solutions. The concluding remarks are given in Section 4.

2. Surface Green's functions

2.1. Normal case

We first consider the normal case in which the concentrated force is applied perpendicular to the surface of the FGM half-plane, as depicted in Figure 1. The half-plane is isotropic, with E and ν being the Young's modulus and Poisson's ratio, respectively, but functionally graded along the x-direction.

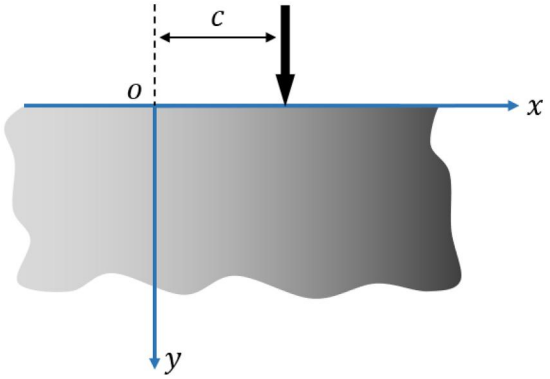

Figure 1. A Normal concentrated force applied on the surface of a horizontally graded half-plane.

The two-dimensional stress-displacement relations can be written as:

$$\begin{cases} \sigma_{xx} = \dfrac{E_\alpha}{1-\nu_\alpha^2}\left(\dfrac{\partial u}{\partial x} + \nu_\alpha \dfrac{\partial v}{\partial y}\right) \\ \sigma_{yy} = \dfrac{E_\alpha}{1-\nu_\alpha^2}\left(\nu_\alpha \dfrac{\partial u}{\partial x} + \dfrac{\partial v}{\partial y}\right) \\ \sigma_{xy} = \dfrac{E_\alpha}{2(1+\nu_\alpha)}\left(\dfrac{\partial u}{\partial y} + \dfrac{\partial v}{\partial x}\right) \end{cases} \tag{1}$$

where σ_{ij} are the stress components; u and v are the displacement components in the x- and y-directions, respectively. E_α and ν_α are the two-dimensional counterparts of E and ν, and given by

$$\begin{cases} E_\alpha = \begin{cases} \dfrac{E}{1-\nu^2} & \text{plane strain} \\ E & \text{plane stress} \end{cases} \\ \nu_\alpha = \begin{cases} \dfrac{\nu}{1-\nu} & \text{plane strain} \\ \nu & \text{plane stress} \end{cases} \end{cases} \tag{2}$$

We consider the case that E_α varies exponentially while ν_α keeps unchanged along the x-direction, i.e.

$$E_\alpha(x) = E_{\alpha 0} e^{\beta x}, \quad \nu_\alpha(x) = \nu_{\alpha 0} \tag{3}$$

where $E_{\alpha 0}$ and $\nu_{\alpha 0}$ are constants, and β is the material gradient index. If $\beta > 0$, the material hardens along the x-direction, while it softens for $\beta < 0$.

Substituting Equation (1) into the equilibrium equations without body forces yields:

$$\begin{cases} 2\dfrac{\partial^2 u}{\partial x^2} + (1-\nu_\alpha)\dfrac{\partial^2 u}{\partial y^2} + (1+\nu_\alpha)\dfrac{\partial^2 v}{\partial x \partial y} + 2\beta\left(\dfrac{\partial u}{\partial x} + \nu_\alpha \dfrac{\partial v}{\partial y}\right) = 0 \\ (1-\nu_\alpha)\dfrac{\partial^2 v}{\partial x^2} + 2\dfrac{\partial^2 v}{\partial y^2} + (1+\nu_\alpha)\dfrac{\partial^2 u}{\partial x \partial y} + \beta(1-\nu_\alpha)\left(\dfrac{\partial u}{\partial y} + \dfrac{\partial v}{\partial x}\right) = 0 \end{cases} \tag{4}$$

In order to write the above governing equations in a more compact form, we may let $A = 2$ and $B = 1 - \nu_\alpha$. Then, we have

$$\begin{cases} Au_{,xx} + Bu_{,yy} + (A-B)v_{,xy} + A\beta\left[u_{,x} + (1-B)v_{,y}\right] = 0 \\ Bv_{,xx} + Av_{,yy} + (A-B)u_{,xy} + B\beta(u_{,y} + v_{,x}) = 0 \end{cases} \tag{5}$$

where a subscript comma indicates partial differentiation with respect to the variable that follows. There is certain symmetry in the coefficients in the second equation of Equation (5), which enables us to rewrite it as:

$$B\frac{\partial}{\partial x}\left(v_{,x}-u_{,y}+A\frac{\beta}{2}v\right)+A\frac{\partial}{\partial y}\left(v_{,y}+u_{,x}+B\frac{\beta}{2}u\right)=0 \tag{6}$$

Then we can introduce a potential function Φ such that

$$\begin{cases} v_{,x}-u_{,y}+A\dfrac{\beta}{2}v=A\dfrac{\partial\Phi}{\partial y} \\ v_{,y}+u_{,x}+B\dfrac{\beta}{2}u=-B\dfrac{\partial\Phi}{\partial x} \end{cases} \tag{7}$$

Substituting Equation (7) into the first equation of Equation (5) gives, together with Equation (7),

$$\begin{cases} v_{,x}-u_{,y}=A\left(\Phi_{,y}-\dfrac{\beta}{2}v\right) \\ v_{,y}+u_{,x}=-B\left(\Phi_{,x}+\dfrac{\beta}{2}u\right) \\ 2\Delta\Phi+(A-B)\beta\left(\Phi_{,x}+\dfrac{\beta}{2}u\right)=0 \end{cases} \tag{8}$$

where $\Delta=\partial_x^2+\partial_y^2$ is the two-dimensional Laplace operator. Appling Fourier transform to Equation (8) with respect to x, the detailed expressions of the transformed displacements U and V can be obtained, and they are given in Appendix A.

Without loss of generality, it is assumed that the concentrated force acts at $x=c$. The boundary conditions and the regularity conditions are:

$$\begin{cases} \sigma_{yy}|_{y=0}=-P\delta(x-c) \\ \sigma_{xy}|_{y=0}=0 \\ u|_{y\to+\infty}=0 \\ v|_{y\to+\infty}=0 \end{cases} \tag{9}$$

Considering the linearity of Fourier transform, it is advisable to perform the inverse Fourier transform on U,V for $y=0$. Then we obtain v at $y=0$ as:

$$\begin{aligned} v|_{y=0}&=\mathsf{F}^{-1}[\mathsf{V}]|_{y=0} \\ &=\frac{P\mathrm{e}^{-\beta c}}{E_{\alpha 0}\pi}\int_{-\infty}^{+\infty}\frac{\sqrt{\omega^2-\mathrm{i}\beta\omega+\beta^2\nu_{\alpha 0}/4}}{\omega(\omega-\mathrm{i}\beta)}\mathrm{e}^{\mathrm{i}\omega(x-c)}\mathrm{d}\omega \end{aligned} \tag{10}$$

The correctness of Equation (10) may be verified by considering the limit $\beta\to 0$ (i.e. for a homogeneous half-plane), for which we have

$$\begin{aligned} v|_{y=0}&=\frac{P}{E_{\alpha 0}\pi}\int_{-\infty}^{+\infty}\frac{\sqrt{\omega^2}}{\omega^2}\mathrm{e}^{\mathrm{i}\omega(x-c)}\mathrm{d}\omega=\frac{P}{E_{\alpha 0}\pi}\int_{-\infty}^{+\infty}\frac{1}{|\omega|}\mathrm{e}^{\mathrm{i}\omega(x-c)}\mathrm{d}\omega \\ &=-\frac{2P}{E_{\alpha 0}\pi}(\ln|x-c|+\gamma) \end{aligned} \tag{11}$$

where γ is the Euler-Mascheroni constant. It is seen that the result in Equation (11) is consistent with the solution of the Boussinesq-Flamant problem in classical elasticity [32].

However, the integration in Equation (10) for $\beta\neq 0$ is very difficult to work out analytically. We therefore change to consider the case of small gradient index for which β^2 is a higher-order small quantity than β, i.e. β^2 can be neglected in Equation (10), resulting in:

$$v|_{y=0}=\frac{P\mathrm{e}^{-\beta c}}{E_{\alpha 0}\pi}\int_{-\infty}^{+\infty}\frac{1}{\sqrt{\omega^2-\mathrm{i}\beta\omega}}\mathrm{e}^{\mathrm{i}\omega(x-c)}\mathrm{d}\omega \tag{12}$$

It is interesting to note that, when the Poisson's ratio is zero, we also get Equation (12) from Equation (10).

The integral in Equation (12) can be written in terms of two parts as:

$$\begin{aligned} \int_{-\infty}^{+\infty}\frac{1}{\sqrt{\omega^2-\mathrm{i}\beta\omega}}\mathrm{e}^{\mathrm{i}\omega(x-c)}\mathrm{d}\omega&=\int_{0}^{+\infty}\frac{1}{\sqrt{\omega^2-\mathrm{i}\beta\omega}}\mathrm{e}^{\mathrm{i}\omega(x-c)}\mathrm{d}\omega \\ &+\int_{-\infty}^{0}\frac{1}{\sqrt{\omega^2-\mathrm{i}\beta\omega}}\mathrm{e}^{\mathrm{i}\omega(x-c)}\mathrm{d}\omega \end{aligned} \tag{13}$$

For the first part, setting $\omega=\rho^2$ gives

$$\begin{aligned} \int_{0}^{+\infty}\frac{1}{\sqrt{\omega^2-\mathrm{i}\beta\omega}}\mathrm{e}^{\mathrm{i}\omega(x-c)}\mathrm{d}\omega&=\int_{0}^{+\infty}\frac{2}{\sqrt{\rho^2-\mathrm{i}\beta}}\mathrm{e}^{\mathrm{i}\rho^2(x-c)}\mathrm{d}\rho \\ &=\int_{0}^{+\infty}\frac{2\mathrm{i}}{\sqrt{(\mathrm{i}\rho)^2+\mathrm{i}\beta}}\mathrm{e}^{\mathrm{i}\rho^2(x-c)}\mathrm{d}\rho \\ &=\int_{0}^{+\infty}\frac{2\sqrt{\mathrm{i}}}{\sqrt{\mathrm{i}\left(\frac{\rho}{\sqrt{\beta}}\right)^2+1}}\mathrm{e}^{\mathrm{i}\left(\frac{\rho}{\sqrt{\beta}}\right)^2[\beta(x-c)]}\mathrm{d}\left(\frac{\rho}{\sqrt{\beta}}\right) \end{aligned} \tag{14}$$

which finally leads to

$$\begin{aligned} &\int_{0}^{+\infty}\frac{1}{\sqrt{\omega^2-\mathrm{i}\beta\omega}}\mathrm{e}^{\mathrm{i}\omega(x-c)}\mathrm{d}\omega \\ &=\frac{1}{2\sqrt{2}\pi}\left\{G_{4,2}^{2,3}\left[\frac{2\mathrm{i}}{\beta|c-x|},\frac{1}{2}\middle|_{\frac{1}{4},\frac{3}{4}}^{\frac{1}{2},1,1,\frac{1}{2}}\right]\right. \\ &\left.-\mathrm{isgn}(c-x)G_{4,2}^{2,3}\left[\frac{2\mathrm{i}}{\beta|c-x|},\frac{1}{2}\middle|_{\frac{1}{4},\frac{3}{4}}^{\frac{1}{2},\frac{1}{2},1,1}\right]\right\} \end{aligned} \tag{15}$$

where $\mathrm{sgn}(x)$ is the signum function, and $G_{p,q}^{m,n}\left[z,r\middle|_{b_1,\ldots,b_q}^{a_1,\ldots,a_p}\right]$ is the Meijer G-function [33]:

$$\begin{aligned} &G_{p,q}^{m,n}\left[z,r\middle|_{b_1,\ldots,b_q}^{a_1,\ldots,a_p}\right] \\ &=\frac{r}{2\pi\mathrm{i}}\int_L\frac{\Gamma(1-a_1-rs)\cdots\Gamma(1-a_n-rs)\Gamma(b_1+rs)\cdots\Gamma(b_m+rs)}{\Gamma(a_{n+1}+rs)\cdots\Gamma(a_p+rs)\Gamma(1-b_{m+1}-rs)\cdots\Gamma(1-b_q-rs)}z^{-s}\mathrm{d}s \end{aligned} \tag{16}$$

and $r\middle|_{b_1,\ldots,b_q}^{a_1,\ldots,a_p}$ are parameters for the Mellin-Barnes type integral in Equation (16).

For the second part in Equation (13), by taking $p=-\omega$, we derive:

$$\int_{-\infty}^{0}\frac{1}{\sqrt{\omega^2-\mathrm{i}\beta\omega}}\mathrm{e}^{\mathrm{i}\omega(x-c)}\mathrm{d}\omega=\int_{0}^{+\infty}\frac{1}{\sqrt{p(p+\mathrm{i}\beta)}}\mathrm{e}^{-\mathrm{i}p(x-c)}\mathrm{d}p \tag{17}$$

On letting $p = h^2$, we have:

$$\int_0^{+\infty} \frac{1}{\sqrt{p(p+\mathrm{i}\beta)}} \mathrm{e}^{-\mathrm{i}p(x-c)} \mathrm{d}p = \int_0^{+\infty} \frac{2}{\sqrt{h^2+\mathrm{i}\beta}} \mathrm{e}^{-\mathrm{i}h^2(x-c)} \mathrm{d}h = \frac{2}{\sqrt{\mathrm{i}}} \int_0^{+\infty} \frac{1}{\sqrt{\frac{1}{\mathrm{i}}\left(\frac{h}{\sqrt{\beta}}\right)^2 + 1}} \mathrm{e}^{-\mathrm{i}\left(\frac{h}{\sqrt{\beta}}\right)^2 [\beta(x-c)]} \mathrm{d}\left(\frac{h}{\sqrt{\beta}}\right) \tag{18}$$

from which we finally get:

$$\begin{aligned} &\int_0^{+\infty} \frac{1}{\sqrt{p(p+\mathrm{i}\beta)}} \mathrm{e}^{-\mathrm{i}p(x-c)} \mathrm{d}p \\ &= K_0\left(\frac{\beta|c-x|}{2}\right)\left[\mathrm{sgn}(c-x)\sinh\left(\frac{\beta|c-x|}{2}\right) + \cosh\left(\frac{\beta|c-x|}{2}\right)\right] \\ &+ \frac{1}{2}\mathrm{i}\pi[\mathrm{sgn}(c-x)-1] I_0\left(\frac{\beta|c-x|}{2}\right)\left[\cosh\left(\frac{\beta|c-x|}{2}\right) - \sinh\left(\frac{\beta|c-x|}{2}\right)\right] \end{aligned} \tag{19}$$

where $I_\mu(\cdot)$ and $K_\mu(\cdot)$ are the modified Bessel functions of the first and second kinds, respectively. The combination of Equations (15) and (19) gives the analytical result of Equation (12), which is for the case of small gradient index.

To further simplify the above analytical solution, especially the terms containing the Meijer G-function, we introduce the following Fox H-function:

$$H_{p,q}^{m,n}\left[z\middle|\begin{matrix}(a_1,\alpha_1),\ldots,(a_p,\alpha_p)\\(b_1,\beta_1),\ldots,(b_q,\beta_q)\end{matrix}\right] = \frac{1}{2\pi\mathrm{i}}\int_L h(s) z^{-s}\mathrm{d}s \tag{20}$$

where

$$h(s) = \frac{\prod_{j=1}^{m}\Gamma(b_j+\beta_j s)\prod_{j=1}^{n}\Gamma(1-a_j-\alpha_j s)}{\prod_{j=m+1}^{q}\Gamma(1-b_j-\beta_j s)\prod_{j=n+1}^{p}\Gamma(a_j+\alpha_j s)} \tag{21}$$

As a special case of the Fox H-function, the Meijer G-function in Equation (16) can be simplified to:

$$\begin{aligned} G_{p,q}^{m,n}\left[z,\frac{1}{2}\middle|\begin{matrix}a_1,\ldots,a_p\\b_1,\ldots,b_q\end{matrix}\right] &= \frac{1}{2}H_{p,q}^{m,n}\left[z\middle|\begin{matrix}\left(a_1,\frac{1}{2}\right),\ldots,\left(a_p,\frac{1}{2}\right)\\\left(b_1,\frac{1}{2}\right),\ldots,\left(b_q,\frac{1}{2}\right)\end{matrix}\right] \\ &= H_{p,q}^{m,n}\left[z^2\middle|\begin{matrix}(a_1,1),\ldots,(a_p,1)\\(b_1,1),\ldots,(b_q,1)\end{matrix}\right] = G_{p,q}^{m,n}\left[z^2\middle|\begin{matrix}a_1,\ldots,a_p\\b_1,\ldots,b_q\end{matrix}\right] \end{aligned} \tag{22}$$

where we have made use of the first property of the Fox H-function as follows:

$$\frac{1}{\kappa}H_{p,q}^{m,n}\left[z\middle|\begin{matrix}(a_1,\alpha_1),\ldots,(a_p,\alpha_p)\\(b_1,\beta_1),\ldots,(b_q,\beta_q)\end{matrix}\right] = H_{p,q}^{m,n}\left[z^\kappa\middle|\begin{matrix}(a_1,\kappa\alpha_1),\ldots,(a_p,\kappa\alpha_p)\\(b_1,\kappa\beta_1),\ldots,(b_q,\kappa\beta_q)\end{matrix}\right] \tag{23}$$

The right-hand side of Equation (15) then can be rewritten as:

$$\frac{1}{2\sqrt{2}\pi}\left\{G_{2,4}^{3,2}\left[-\frac{\beta^2(c-x)^2}{4}\middle|\begin{matrix}\frac{3}{4},\frac{1}{4}\\\frac{1}{2},0,0,\frac{1}{2}\end{matrix}\right] - \mathrm{isgn}(c-x)G_{2,4}^{3,2}\left[-\frac{\beta^2(c-x)^2}{4}\middle|\begin{matrix}\frac{3}{4},\frac{1}{4}\\\frac{1}{2},\frac{1}{2},0,0\end{matrix}\right]\right\} \tag{24}$$

The following second property of the Fox H-function have also been noticed:

$$H_{p,q}^{m,n}\left[z\middle|\begin{matrix}(a_1,\alpha_1),\ldots,(a_p,\alpha_p)\\(b_1,\beta_1),\ldots,(b_q,\beta_q)\end{matrix}\right] = H_{q,p}^{n,m}\left[\frac{1}{z}\middle|\begin{matrix}(1-b_1,\beta_1),\ldots,(1-b_q,\beta_q)\\(1-a_1,\alpha_1),\ldots,(1-a_p,\alpha_p)\end{matrix}\right] \tag{25}$$

where $\arg(1/z) = -\arg(z)$. Now the results in Equation (24) can be further simplified to:

$$G_{2,4}^{3,2}\left[-\frac{\beta^2(c-x)^2}{4}\middle|\begin{matrix}\frac{3}{4},\frac{1}{4}\\\frac{1}{2},0,0,\frac{1}{2}\end{matrix}\right] = \left[2\sqrt{2}\pi K_0\left(\frac{\beta(c-x)}{2}\right)\cosh\left(\frac{\beta(c-x)}{2}\right) + \mathrm{i}\sqrt{2}\pi^2\mathrm{sgn}(c-x) I_0\left(\frac{\beta(c-x)}{2}\right)\left(\sinh\left(\frac{\beta(c-x)}{2}\right) - \cosh\left(\frac{\beta(c-x)}{2}\right)\right)\right]^* \tag{26}$$

$$\begin{aligned} &G_{2,4}^{3,2}\left[-\frac{\beta^2(c-x)^2}{4}\middle|\begin{matrix}\frac{3}{4},\frac{1}{4}\\\frac{1}{2},\frac{1}{2},0,0\end{matrix}\right] \\ &= \left[-2\sqrt{2}\pi\mathrm{isgn}(c-x)K_0\left(\frac{\beta(c-x)}{2}\right)\sinh\left(\frac{\beta(c-x)}{2}\right) + \sqrt{2}\pi^2 I_0\left(\frac{\beta(c-x)}{2}\right)\left(\cosh\left(\frac{\beta(c-x)}{2}\right) - \sinh\left(\frac{\beta(c-x)}{2}\right)\right)\right]^* \end{aligned} \tag{27}$$

where $[\cdot]^*$ represents the complex conjugation, and $|c-x| = (c-x)\mathrm{sgn}(c-x)$, $\mathrm{sgn}^2(c-x) = 1$. The occurrence of complex conjugation is due to the negative sign before $\arg(\cdot)$ as indicated below Equation (25). The imaginary parts in Equations (15) and (19) will cancel each other out in Equation (13).

The analytical expression for the horizontal displacement at $y = 0$ can be derived through inverse Fourier transform of U in Appendix A even without the weak gradient assumption. The result is

$$\begin{aligned} u|_{y=0} &= \mathsf{F}^{-1}[\mathsf{U}]|_{y=0} = \frac{P\mathrm{e}^{-\beta c}}{2\pi E_{\alpha 0}}\int_{-\infty}^{+\infty}\frac{\mathrm{i}(1-\nu_{\alpha 0})\omega - \beta\nu_{\alpha 0}}{\omega(\omega-\mathrm{i}\beta)}\mathrm{e}^{\mathrm{i}\omega(x-c)}\mathrm{d}\omega \\ &= -\frac{P}{2E_{\alpha 0}}\left[2\mathrm{e}^{-\beta x}\mathsf{H}(x-c) + \nu_{\alpha 0}\mathrm{e}^{-\beta c}\mathrm{sgn}(c-x)\right] \end{aligned} \tag{28}$$

where $\mathsf{H}(x)$ is the Heaviside step function.

2.2. Tangential case

The problem of a tangential concentrated force acting on the surface of the horizontally graded half-plane is depicted in Figure 2.

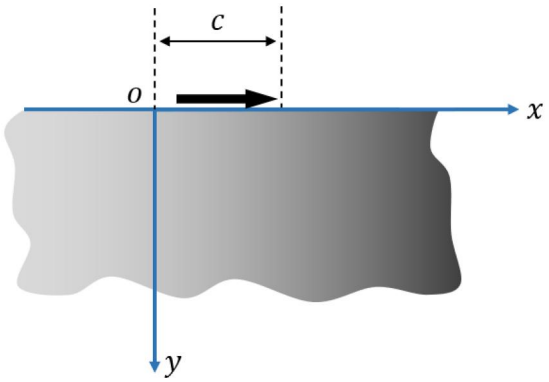

Figure 2. A tangential concentrated force applied on the surface of a horizontally graded half-plane.

For the tangential case, all the basic equations in Section 2.1 remain the same, except for the boundary conditions, which now read as:

$$\begin{cases} \sigma_{yy}|_{y=0} = 0 \\ \sigma_{xy}|_{y=0} = -Q\delta(x-c) \\ u|_{y\to+\infty} = 0 \\ v|_{y\to+\infty} = 0 \end{cases} \tag{29}$$

Following the same procedure as for Equation (10), the vertical displacement at $y = 0$ under the tangential concentrated force can be obtained, also without the weak gradient assumption:

$$\begin{aligned} v|_{y=0} &= \mathsf{F}^{-1}[\mathsf{V}]|_{y=0} = -\frac{Q\mathrm{e}^{-\beta c}}{2\pi E_{\alpha 0}}\int_{-\infty}^{+\infty}\frac{\mathrm{i}(1-\nu_{\alpha 0})\omega+\beta}{\omega(\omega-\mathrm{i}\beta)}\mathrm{e}^{\mathrm{i}\omega(x-c)}\mathrm{d}\omega \\ &= -\frac{Q}{2E_{\alpha 0}}\left[2\nu_{\alpha 0}\mathrm{e}^{-\beta x}\mathsf{H}(x-c)+\mathrm{e}^{-\beta c}\mathrm{sgn}(c-x)\right] \end{aligned} \tag{30}$$

The correctness of the above solution may also be checked by considering the limit $\beta \to 0$, for which we arrive at

$$\begin{aligned} v|_{y=0} &= \mathsf{F}^{-1}[\mathsf{V}]|_{y=0} = -\frac{Q}{2\pi E_{\alpha 0}}\int_{-\infty}^{+\infty}\frac{\mathrm{i}(1-\nu_{\alpha 0})}{\omega}\mathrm{e}^{\mathrm{i}\omega(x-c)}\mathrm{d}\omega \\ &= \frac{Q(1-\nu_{\alpha 0})}{2E_{\alpha 0}}\mathrm{sgn}(x-c) \end{aligned} \tag{31}$$

which is the classical solution for a homogeneous half-plane.

The horizonal displacement at $y = 0$ is:

$$u|_{y=0} = \mathsf{F}^{-1}[\mathsf{U}]|_{y=0} = \frac{Q\mathrm{e}^{-\beta c}}{E_{\alpha 0}\pi}\int_{-\infty}^{+\infty}\frac{\sqrt{\omega^2-\mathrm{i}\beta\omega+\beta^2\nu_{\alpha 0}/4}}{\omega(\omega-\mathrm{i}\beta)}\mathrm{e}^{\mathrm{i}\omega(x-c)}\mathrm{d}\omega \tag{32}$$

Under the weak gradient assumption, Equation (32) is just the same as Equation (10), expect for the value of the concentrated force, which can be proved according to the reciprocity theorem of work. Thus, the methodologies there can also be applied to Equation (32), which is omitted here.

3. Numerical results and discussions

3.1. Numerical results

Let $E_{\alpha 0} = 1$ (Pa), $c = 0$ (m), $\beta = 0.1$, $\nu = 0.25$, $P = 1$ (N), $Q = 1$ (N). The corresponding numerical results for the surface normal and tangential displacements (in the vertical and horizontal directions, respectively) are as follows respectively.

The singularity due to the concentrated force and the asymmetry (with respect to the y-axis) due to the gradient of material are both clearly shown by the numerical results as given in Figures 3 and 4. It is also noted that, the displacements don't tend to be zero while $x \to +\infty$. This phenomenon also appears for a homogeneous half-plane [32].

3.2. Comparison with finite element analysis

The analytical solutions are also verified here through comparing their numerical results with simulations by the finite element method. The problem domain is a half-plane, however, we usually do not make the computational domain infinite in finite element analysis (FEA). In order to simulate the infinite condition, an appropriate large elastic plane is selected, and the fixed conditions at the bottom and both ends are adopted. The FEA results therefore will not be identically the same as the developed analytical solutions, especially near the boundaries.

In order to compare with the FEA results, we need to introduce the following conditions in the analytical solutions to eliminate the undetermined surface sedimentation therein:

$$u|_{x\to+\infty} = 0, \quad v|_{x\to+\infty} = 0 \tag{33}$$

As can be seen from the Figures 5 and 6, the FEA results also reflect the asymmetry with respect to the y-axis. The meshes after deformation are significantly distorted near the point where the concentrated force acts, which indicates the singularity in the field.

Moreover, as is known to all, the singularity caused by the concentrated force at its application point cannot be captured by the common FEA, which differs from the analytical solutions. Thus, only at a point away from the force

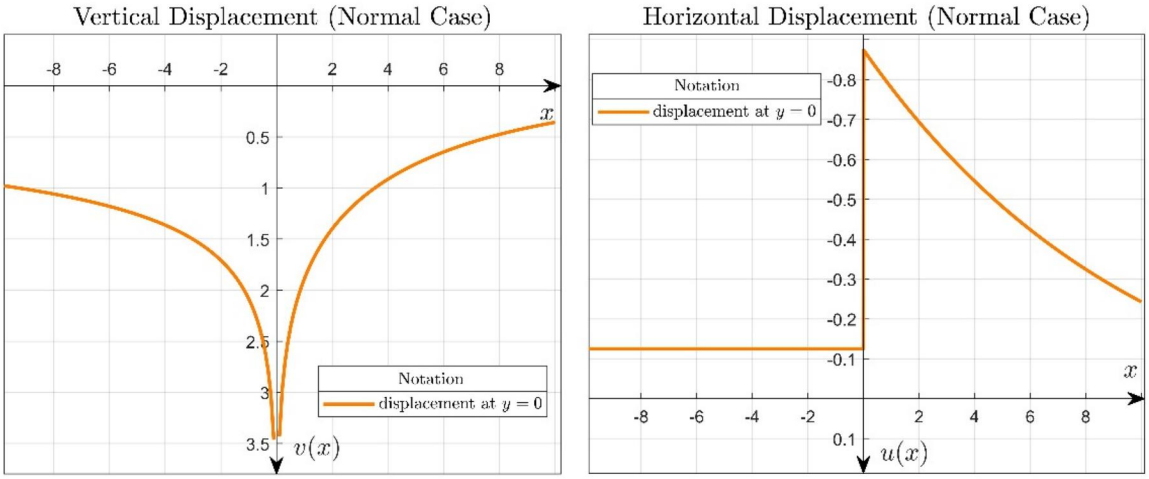

Figure 3. Surface displacements under a normal concentrated force P at the origin.

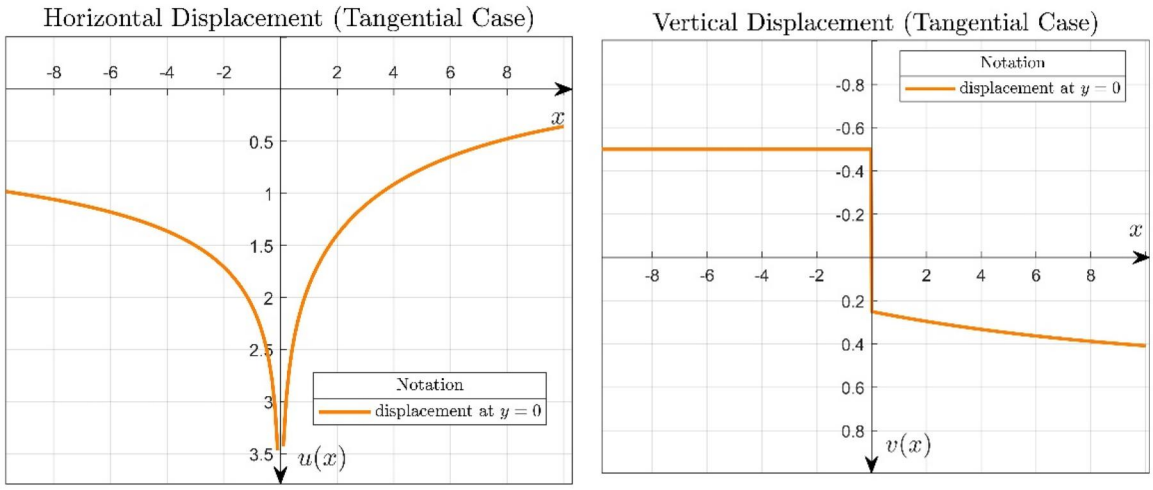

Figure 4. Surface displacements under a tangential concentrated force Q at the origin.

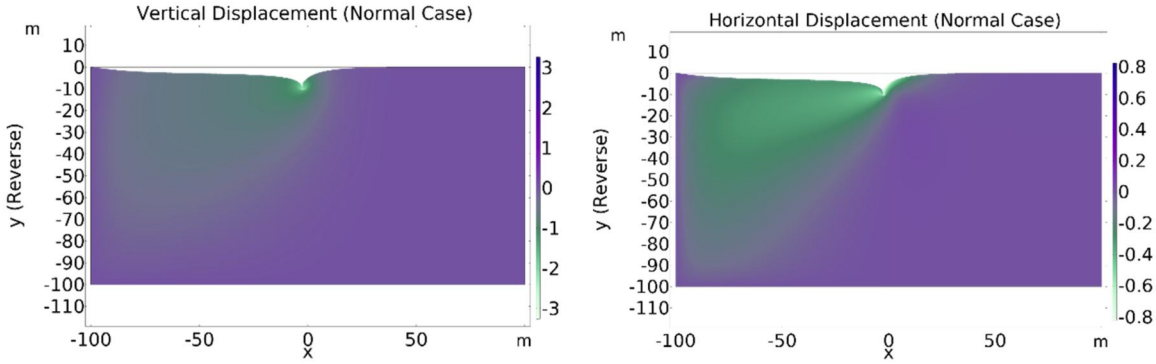

Figure 5. FEA results for the normal force with deformation scale factor 4.52 and 2148 nodes. Deformation scale factor consists in scaling the displacement amplitude for visualizing a deformed mesh image.

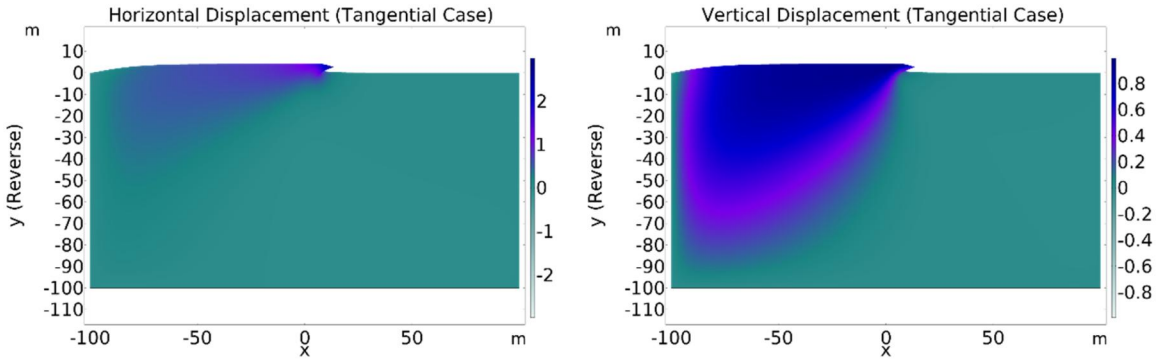

Figure 6. FEA results for the tangential force with deformation scale factor 4.52 and 2148 nodes.

as well as the lateral boundaries, the comparison is meaningful. We make the comparisons in Figures 7 and 8 for the normal and tangential forces, respectively. Three different sizes, i.e. 200×100, 500×100, and 2000×100 (in meters), of the problem domain are adopted in FEA simulations, to study the size effect of the FEA model on the displacements.

The FEA results are basically consistent with the analytical solutions. In particular, when the size of the FEA model increases, the results approach the exact solutions, indicating a quite stable convergence behavior.

To show the distribution of the absolute error of displacement, some problematic regions are excluded (i.e. near the force application point and lateral boundary), and only the region $[-80, -20] \cup [20, 80]$ is considered. The absolute errors between the FEA results and the analytical solutions are then shown in Figures 9 and 10, wherein spline fitting is performed to ensure curve smoothness.

The mean square errors (MSEs) of the FEA results for three different sizes of the model, as compared to the analytical solutions, are shown in Table 1 below. The MSE is defined as

$$\mathrm{MSE} = \frac{1}{n}\sum_{i=1}^{n}(\hat{y}_i - y_i)^2 \tag{34}$$

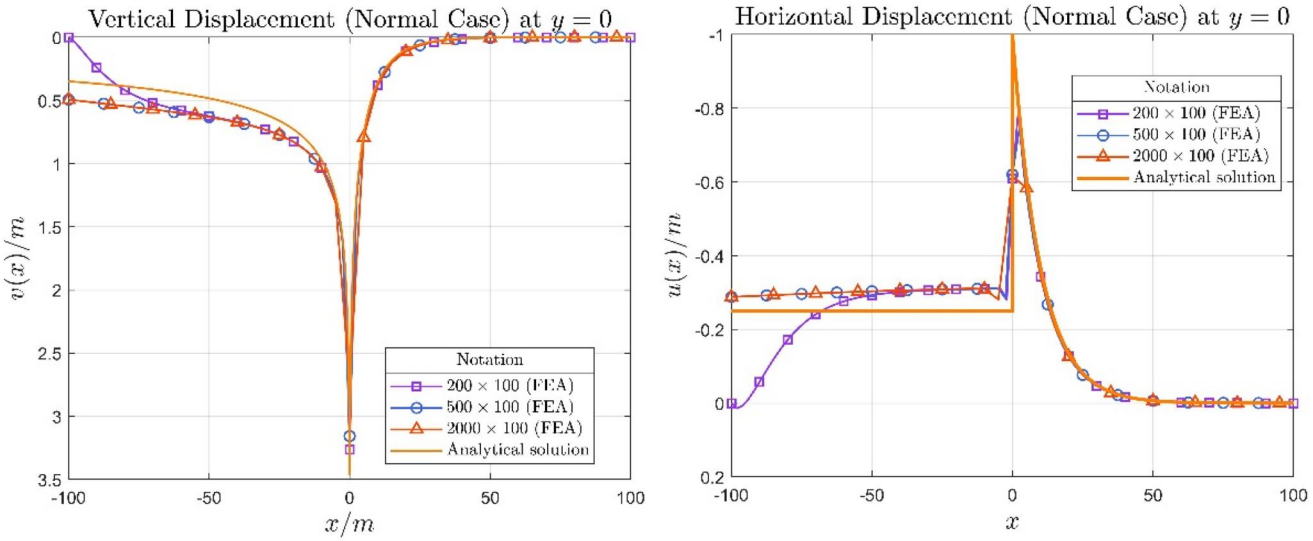

Figure 7. Comparison between FEA results and analytical solutions in the normal case.

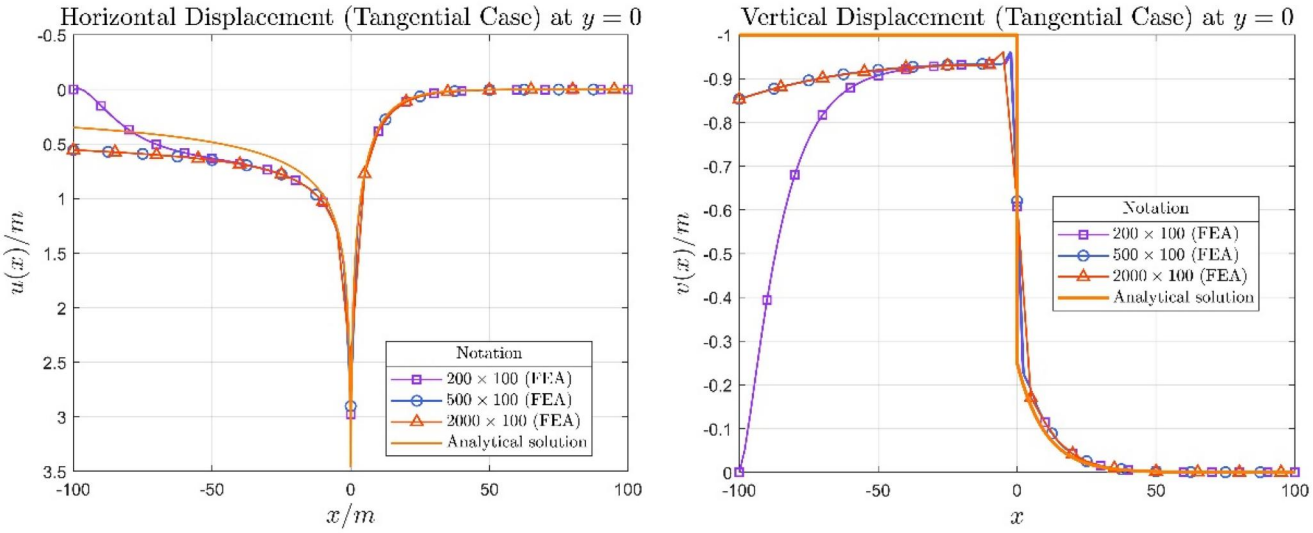

Figure 8. Comparison between FEA results and analytical solutions in the tangential case.

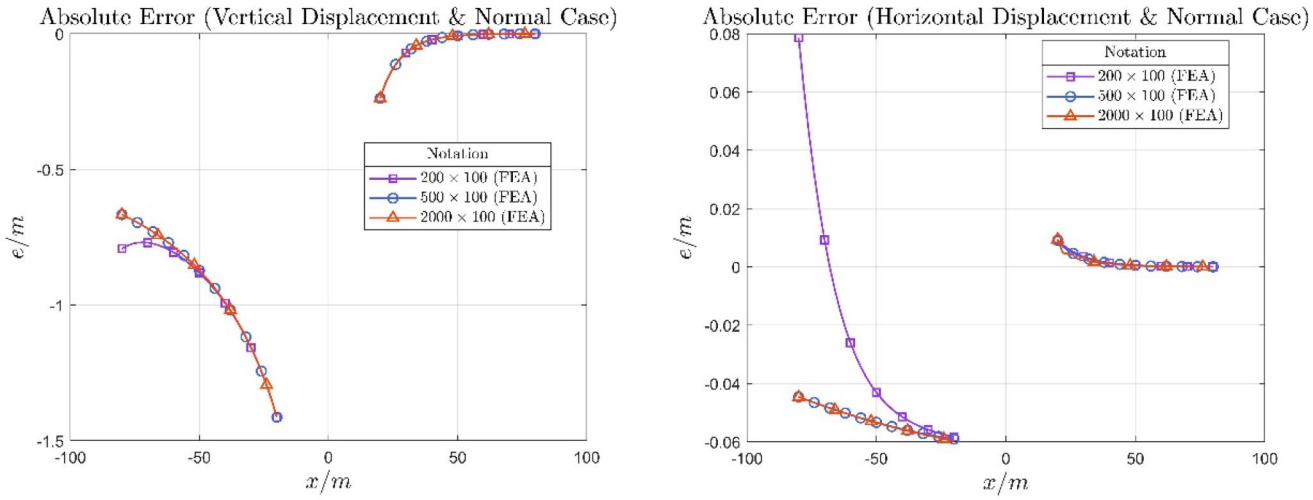

Figure 9. Absolute error for different sizes of the FEA model in the normal case.

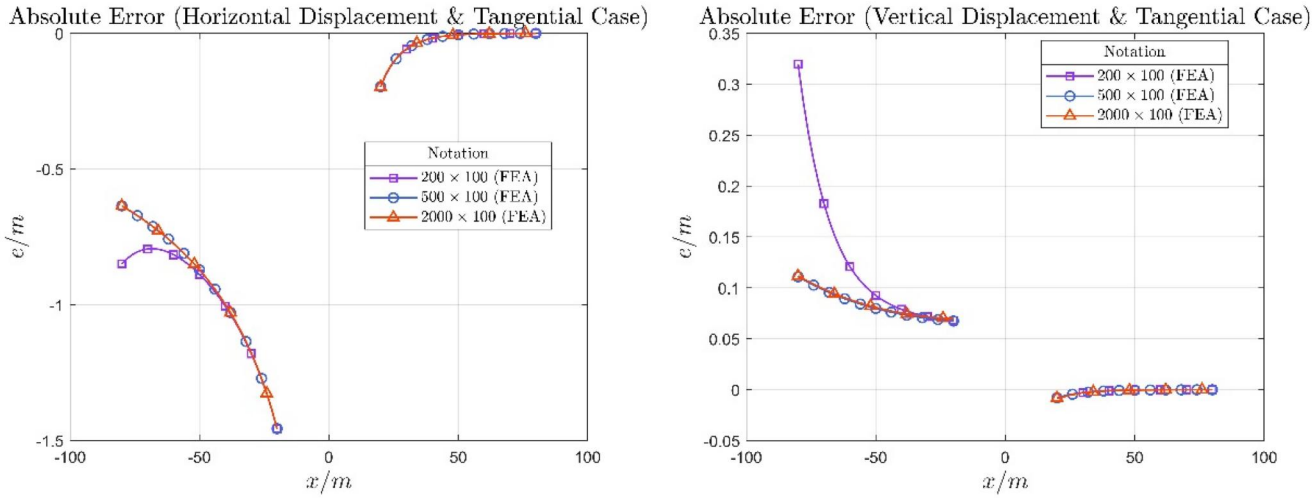

Figure 10. Absolute error for different sizes of the FEA model in the tangential case.

Table 1. Mean square errors (m^2) of the FEA results for three different model sizes.

	Vertical Displacement (Normal Case)	Horizontal Displacement (Normal Case)	Vertical Displacement (Tangential Case)	Horizontal Displacement (Tangential Case)
$MSE_{200\times100}$	4.73×10^{-1}	1.05×10^{-3}	9.87×10^{-3}	4.93×10^{-1}
$MSE_{500\times100}$	4.54×10^{-1}	1.41×10^{-3}	3.54×10^{-3}	4.59×10^{-1}
$MSE_{2000\times100}$	4.54×10^{-1}	1.41×10^{-3}	3.64×10^{-3}	4.59×10^{-1}

where n is sample size, $\hat{y}_i$ is the predicted displacement in the analytical solutions, and y_i is the displacement in the FEA results.

It can be seen from Table 1 that the MSEs between the FEA results and the analytical solutions are small, again confirming that the derived analytical solutions are correct. It is worth noting that, the FEA result of displacement over the region with a large material stiffness (i.e. $[20, 80]$) is more accurate than that over the region with a small material stiffness (i.e. $[-80, -20]$).

4. Conclusions

This investigation delves into the intricacies of the deformation problem of an elastic half-plane with specific horizontal material gradient under the action of a concentrated force. The governing equations are simplified by introducing appropriate potential functions, and the analytical surface Green's functions for both normal and tangential concentrated forces are obtained by the Fourier transform technique.

For the normal force, the surface vertical displacement is derived under the assumption of weak gradient. The Meijer G-function and the Fox H-function are incorporated into the solution, not only for facilitating the mathematical derivation, but also for simplifying the final expression. The surface horizontal displacement is also derived, but in a more straightforward way. For the tangential force, the solution is obtained similarly. It is noted that the analytical solutions all reveal essential features (such as singularity and asymmetry), and can be reduced to the classical Boussinesq-Flamant solutions for a homogeneous half-plane.

To verify the analytical solutions of surface Green's functions, FEA simulations are carried out. The two methods yield essentially identical results, particularly at a point away from the concentrated force where singularity exists. The agreement confirms the correctness of the derived analytical expressions, which establish a platform for subsequent research endeavors such as contact analysis of FGM half-planes under the action of rigid indenter.

Disclosure statement

No potential conflict of interest was reported by the author(s).

Funding

The work was supported by the National Natural Science Foundation of China (Nos. 12192211 and 12192210), the Natural Science Foundation of Zhejiang Province (No. LD21A020001), and the 111 Project, PR China (No. B21034). This work was also partly supported by the specialized research projects of Huanjiang Laboratory, Zhuji, Zhejiang Province.

ORCID

Weiqiu Chen http://orcid.org/0000-0003-0655-3303

References

[1] X.D. Xiang, X. Sun, G. Briceño, Y. Lou, K.A. Wang, H. Chang, W.G. Wallace-freedman, S.W. Chen, and P.G. Schultz, A combinatorial approach to materials discovery, Science, vol. 268, no. 5218, pp. 1738–1740, 1995. DOI: 10.1126/science.268.5218.1738.

[2] J.J. De Pablo, N.E. Jackson, M.A. Webb, L.Q. Chen, J.E. Moore, D. Morgan, R. Jacobs, T. Pollock, D.G. Schlom, E.S. Toberer, J. Analytis, I. Dabo, D.M. DeLongchamp, G.A. Fiete, G.M. Grason,

G. Hautier, Y. Mo, K. Rajan, E.J. Reed, E. Rodriguez, V. Stevanovic, J. Suntivich, K. Thornton, and J.C. Zhao, New frontiers for the materials genome initiative, Npj Comput. Mater., vol. 5, no. 1, pp. 41, 2019. DOI: 10.1038/s41524-019-0173-4.

[3] A. Khosravani, A. Cecen, and S.R. Kalidindi, Development of high throughput assays for establishing process-structure-property linkages in multiphase polycrystalline metals: application to dual-phase steels, Acta Mater., vol. 123, pp. 55–69, 2017. DOI: 10.1016/j.actamat.2016.10.033.

[4] Z. Zhong, L. Wu, and W. Chen, Progress in the study of mechanics problems of functionally graded materials and structures, Adv. Mech., vol. 40, no. 5, pp. 528–541, 2010. DOI: 10.3788/gzxb20103908.1438.

[5] S. Suresh, and A. Mortensen, Fundamentals of Functionally Graded Materials: Processing and Thermomechanical Behaviour of Graded Metals and Metal-Ceramic Composites, IOM Communications Ltd., London, 1997.

[6] S. Suresh, Graded materials for resistance to contact deformation and damage, Science, vol. 292, no. 5526, pp. 2447–2451, 2001. DOI: 10.1126/science.1059716.

[7] O. Jørgensen, A.E. Giannakopoulos, and S. Suresh, Spherical indentation of composite laminates with controlled gradients in elastic anisotropy, Int. J. Solids Struct., vol. 35, no. 36, pp. 5097–5113, 1998. DOI: 10.1016/S0020-7683(97)00209-6.

[8] D.C. Pender, N.P. Padture, A.E. Giannakopoulos, and S. Suresh, Gradients in elastic modulus for improved contact-damage resistance. Part I: the silicon nitride–oxynitride glass system, Acta Mater., vol. 49, no. 16, pp. 3255–3262, 2001. DOI: 10.1016/S1359-6454(01)00200-2.

[9] L.-L. Ke, and Y.-S. Wang, Fretting contact of two dissimilar elastic bodies with functionally graded coatings, Mech. Adv. Mater. Struct., vol. 17, no. 6, pp. 433–447, 2010. DOI: 10.1080/15376494.2010.483327.

[10] N.A. Rostovtsev, On the theory of elasticity of a nonhomoqeneous medium, Appl. Math. Mech., vol. 28, no. 4, pp. 745–757, 1964. DOI: 10.1016/0021-8928(64)90060-7.

[11] R.E. Gibson, P.T. Brown, and K.R.F. Andrews, Some results concerning displacements in a non-homogeneous elastic layer, Journal of Applied Mathematics and Physics (ZAMP)., vol. 22, no. 5, pp. 855–864, 1971. DOI: 10.1007/BF01591813.

[12] P.T. Brown, and R.E. Gibson, Surface Settlement of a Deep Elastic Stratum Whose Modulus Increases Linearly with Depth, Can. Geotech. J., vol. 9, no. 4, pp. 467–476, 1972. DOI: 10.1139/t72-045.

[13] J.R. Booker, N.P. Balaam, and E.H. Davis, The behaviour of an elastic non-homogeneous half-space. Part I-line and point loads, Num. Anal. Meth. Geomechanics., vol. 9, no. 4, pp. 353–367, 1985. DOI: 10.1002/nag.1610090405.

[14] A. D. de Pater and J. J. Kalker, Eds., The Mechanics of the Contact between Deformable Bodies, Delft University Press, Amsterdam, 1975.

[15] A.E. Giannakopoulos, and S. Suresh, Indentation of solids with gradients in elastic properties: part I. Point force, Int. J. Solids Struct., vol. 34, no. 19, pp. 2357–2392, 1997. DOI: 10.1016/S0020-7683(96)00171-0.

[16] A.E. Giannakopoulos, and S. Suresh, Indentation of solids with gradients in elastic properties: part II. axisymmetric indentors, Int. J. Solids Struct., vol. 34, no. 19, pp. 2393–2428, 1997. DOI: 10.1016/S0020-7683(96)00172-2.

[17] A. Giannakopoulos, Two-dimensional contact analysis of elastic graded materials, J. Mech. Phys. Solids., vol. 48, no. 8, pp. 1597–1631, 2000. DOI: 10.1016/S0022-5096(99)00068-X.

[18] M. Heß, and Q. Li, Tangential contacts of three-dimensional power-law graded elastic solids: a general theory and application to partial slip, Mech. Adv. Mater. Struct., 2023. DOI: 10.1080/15376494.2023.2222289.

[19] M.A. Guler, and F. Erdogan, Contact mechanics of graded coatings, Int. J. Solids Struct., vol. 41, no. 14, pp. 3865–3889, 2004. DOI: 10.1016/j.ijsolstr.2004.02.025.

[20] M.A. Guler, and F. Erdogan, Contact mechanics of two deformable elastic solids with graded coatings, Mech. Mater., vol. 38, no. 7, pp. 633–647, 2006. DOI: 10.1016/j.mechmat.2005.11.006.

[21] M.A. Guler, and F. Erdogan, The frictional sliding contact problems of rigid parabolic and cylindrical stamps on graded coatings, Int. J. Mech. Sci., vol. 49, no. 2, pp. 161–182, 2007. DOI: 10.1016/j.ijmecsci.2006.08.006.

[22] L.-L. Ke, and Y.-S. Wang, Two-dimensional contact mechanics of functionally graded materials with arbitrary spatial variations of material properties, Int. J. Solids Struct., vol. 43, no. 18-19, pp. 5779–5798, 2006. DOI: 10.1016/j.ijsolstr.2005.06.081.

[23] S. Chen, C. Yan, P. Zhang, and H. Gao, Mechanics of adhesive contact on a power-law graded elastic half-space, J. Mech. Phys. Solids., vol. 57, no. 9, pp. 1437–1448, 2009. DOI: 10.1016/j.jmps.2009.06.006.

[24] S. Chen, C. Yan, and A. Soh, Adhesive behavior of two-dimensional power-law graded materials, Int. J. Solids Struct., vol. 46, no. 18–19, pp. 3398–3404, 2009. DOI: 10.1016/j.ijsolstr.2009.05.006.

[25] X. Guo, F. Jin, and H. Gao, Mechanics of non-slipping adhesive contact on a power-law graded elastic half-space, Int. J. Solids Struct., vol. 48, no. 18, pp. 2565–2575, 2011. DOI: 10.1016/j.ijsolstr.2011.05.008.

[26] F. Jin, and X. Guo, Non-slipping adhesive contact of a rigid cylinder on an elastic power-law graded half-space, Int. J. Solids Struct., vol. 47, no. 11–12, pp. 1508–1521, 2010. DOI: 10.1016/j.ijsolstr.2010.02.010.

[27] F. Jin, and X. Guo, Mode-mixity-dependent adhesion of power-law graded elastic solids under normal load and substrate stretch-induced mismatch strain, Int. J. Solids Struct., vol. 49, no. 17, pp. 2349–2357, 2012. DOI: 10.1016/j.ijsolstr.2012.05.003.

[28] İ. Çömez, M.A. Güler, and S. El-Borgi, Continuous and discontinuous contact problems of a functionally graded piezoelectric layer resting on a homogeneous piezoelectric half plane, Mech. Adv. Mater. Struct., vol. 31, no. 10, pp. 2130–2143, 2024. DOI: 10.1080/15376494.2022.2151673.

[29] S. Dag, M.A. Guler, B. Yildirim, and A. Cihan Ozatag, Sliding frictional contact between a rigid punch and a laterally graded elastic medium, Int. J. Solids Struct., vol. 46, no. 22-23, pp. 4038–4053, 2009. DOI: 10.1016/j.ijsolstr.2009.07.023.

[30] S. Dag, Consideration of spatial variation of the friction coefficient in contact mechanics analysis of laterally graded materials: contact mechanics analysis of laterally graded materials, Z Angew. Math. Mech., vol. 96, no. 1, pp. 121–136, 2016. DOI: 10.1002/zamm.201400116.

[31] S. Dag, M.A. Guler, B. Yildirim, and A.C. Ozatag, Frictional Hertzian contact between a laterally graded elastic medium and a rigid circular stamp, Acta Mech., vol. 224, no. 8, pp. 1773–1789, 2013. DOI: 10.1007/s00707-013-0844-z.

[32] S.P. Timoshenko, and J.N. Goodier, Theory of Elasticity, McGraw-Hill, New York, 1988.

[33] A.M. Mathai, A Handbook of Generalized Special Functions for Statistical and Physical Sciences, Clarendon Press, Oxford, 1993.

Appendix A

In this article, the Fourier transform pair is chosen as:

$$\begin{cases} \mathsf{F}^{-1}[F(\omega)] = f(x) = \displaystyle\int_{-\infty}^{+\infty} F(\omega)\mathrm{e}^{\mathrm{i}\omega x}\mathrm{d}\omega \\ \mathsf{F}[f(x)] = F(\omega) = \dfrac{1}{2\pi}\displaystyle\int_{-\infty}^{+\infty} f(\omega)\mathrm{e}^{-\mathrm{i}\omega x}\mathrm{d}x \end{cases} \tag{A1}$$

The expressions of U and V are:

$$\begin{aligned} \mathsf{U} = {} & \frac{\cosh\left(\frac{1}{2}\beta\sqrt{\nu_{\alpha 0}}y\right)}{2\sqrt{\beta^2\nu_{\alpha 0} - 4\mathrm{i}\beta\omega + 4\omega^2}}\left\{2c_1\sqrt{\beta^2\nu_{\alpha 0} - 4\mathrm{i}\beta\omega + 4\omega^2}\cosh\left(\frac{1}{2}y\sqrt{\beta^2\nu_{\alpha 0} - 4\mathrm{i}\beta\omega + 4\omega^2}\right)\right. \\ & \left. + \{c_2[\beta(\nu_{\alpha 0}+3) + 4\mathrm{i}\omega] + 2c_4(\nu_{\alpha 0}-3)\}\sinh\left(\frac{1}{2}y\sqrt{\beta^2\nu_{\alpha 0} - 4\mathrm{i}\beta\omega + 4\omega^2}\right)\right\} \\ & - \frac{\sinh\left(\frac{1}{2}\beta\sqrt{\nu_{\alpha 0}}y\right)}{2\beta\sqrt{\nu_{\alpha 0}}\sqrt{\beta^2\nu_{\alpha 0} - 4\mathrm{i}\beta\omega + 4\omega^2}}\left\{[\beta c_2(\nu_{\alpha 0}-1) + 2c_4(\nu_{\alpha 0}+1)]\sqrt{\beta^2\nu_{\alpha 0} - 4\mathrm{i}\beta\omega + 4\omega^2}\cosh\left(\frac{1}{2}y\sqrt{\beta^2\nu_{\alpha 0} - 4\mathrm{i}\beta\omega + 4\omega^2}\right)\right. \\ & \left. - 2\{\beta c_1[\beta\nu_{\alpha 0} + \mathrm{i}(\nu_{\alpha 0}-1)\omega] + 2c_3\omega[2\mathrm{i}\beta\nu_{\alpha 0} - (1+\nu_{\alpha 0})\omega]\}\sinh\left(\frac{1}{2}y\sqrt{\beta^2\nu_{\alpha 0} - 4\mathrm{i}\beta\omega + 4\omega^2}\right)\right\} \end{aligned} \tag{A2}$$

$$\begin{aligned} \mathsf{V} = {} & \frac{1}{4\beta\sqrt{\nu_{\alpha 0}}\sqrt{\beta^2\nu_{\alpha 0} - 4\mathrm{i}\beta\omega + 4\omega^2}}\left\{2\left[\beta c_2\sqrt{\nu_{\alpha 0}}\sqrt{\beta^2\nu_{\alpha 0} - 4\mathrm{i}\beta\omega + 4\omega^2} + \beta^2 c_2 + \beta(\nu_{\alpha 0}-1)(2c_4\text{-}\mathrm{i}c_2\omega) - 2\mathrm{i}c_4(\nu_{\alpha 0}+1)\omega\right]\right. \\ & \cosh\left[\frac{1}{2}y\left(-\beta\sqrt{\nu_{\alpha 0}} + \sqrt{\beta^2\nu_{\alpha 0} - 4\mathrm{i}\beta\omega + 4\omega^2}\right)\right] \\ & + 2\left\{\beta c_2\sqrt{\nu_{\alpha 0}}\sqrt{\beta^2\nu_{\alpha 0} - 4\mathrm{i}\beta\omega + 4\omega^2} - \beta c_2[\beta\text{-}\mathrm{i}(\nu_{\alpha 0}-1)\omega] + 2c_4[\beta(1-\nu_{\alpha 0}) + \mathrm{i}(\nu_{\alpha 0}+1)\omega]\right\}\cosh\left[\frac{1}{2}y\left(\beta\sqrt{\nu_{\alpha 0}} + \sqrt{\beta^2\nu_{\alpha 0} - 4\mathrm{i}\beta\omega + 4\omega^2}\right)\right] \\ & + \frac{\left(\beta\sqrt{\nu_{\alpha 0}} + \sqrt{\beta^2\nu_{\alpha 0} - 4\mathrm{i}\beta\omega + 4\omega^2}\right)}{\beta + \mathrm{i}\omega}\sinh\left[\frac{1}{2}y\left(\beta\sqrt{\nu_{\alpha 0}} + \sqrt{\beta^2\nu_{\alpha 0} - 4\mathrm{i}\beta\omega + 4\omega^2}\right)\right]\left\{\beta(c_1+2c_3)\sqrt{\nu_{\alpha 0}}\sqrt{\beta^2\nu_{\alpha 0} - 4\mathrm{i}\beta\omega + 4\omega^2}\right. \\ & \left. - \left[\beta^2(2c_3\nu_{\alpha 0} + c_1)\right] + \mathrm{i}\beta\omega[c_1(\nu_{\alpha 0}-1) + 2c_3(\nu_{\alpha 0}+1)] - 2c_3(\nu_{\alpha 0}+1)\omega^2\right\} \\ & + \frac{2\sinh\left[\frac{1}{2}y\left(-\beta\sqrt{\nu_{\alpha 0}} + \sqrt{\beta^2\nu_{\alpha 0} - 4\mathrm{i}\beta\omega + 4\omega^2}\right)\right]}{\beta\sqrt{\nu_{\alpha 0}} - \sqrt{\beta^2\nu_{\alpha 0} - 4\mathrm{i}\beta\omega + 4\omega^2}}\left\{\beta^3 c_1(\nu_{\alpha 0}-1)\nu_{\alpha 0} + \beta^2\left(2\mathrm{i}\omega[-2c_1\nu_{\alpha 0} + c_3(\nu_{\alpha 0}-1)\nu_{\alpha 0} + c_1] - c_1(\nu_{\alpha 0}-1)\sqrt{\nu_{\alpha 0}}\sqrt{\beta^2\nu_{\alpha 0} - 4\mathrm{i}\beta\omega + 4\omega^2}\right)\right. \\ & \left. + 2\beta\omega\left[-\mathrm{i}\sqrt{\nu_{\alpha 0}}(c_3(\nu_{\alpha 0}-1) - c_1)\sqrt{\beta^2\nu_{\alpha 0} - 4\mathrm{i}\beta\omega + 4\omega^2} + c_1(\nu_{\alpha 0}-1)\omega + 2c_3(\nu_{\alpha 0}+1)\omega\right] + 4\mathrm{i}c_3(\nu_{\alpha 0}+1)\omega^3\right\}\Bigg\} \end{aligned} \tag{A3}$$

where c_1, c_2, c_3, c_4 are arbitrary constants, which may be determined by boundary conditions.